ACS OMEGA

http://pubs.acs.org/journal/acsodf

Article

Bacitracin-Engineered BSA/ICG Nanocomplex with Enhanced Photothermal and Photodynamic Antibacterial Activity

Yueying Xu,† Wenhong Zhou,† Le Xiao,† Qian Lan, Mingen Li, Yun Liu, Lijun Song,* and Li Li*

Cite This: *ACS Omega* 2022, 7, 33821−33829

Read Online

ACCESS | Metrics & More | Article Recommendations | Supporting Information

ABSTRACT: To reduce the drug resistance of bacteria and enhance the antibacterial ability in bacterial infection therapy, we designed a new antibacterial nanoagent. In this system, a photosensitizer (indocyanine green, ICG) was loaded in bovine serum albumin (BSA) through hydrophobic-interaction-induced self-assembly to form stable BSA@ICG nanoparticles. Furthermore, a positively charged antibacterial peptide bacitracin (Bac) was physically immobilized onto the surface of BSA@ICG to generate a bacterial-targeted nanomedicine BSA@ICG@Bac through electrostatic interactions. Afterward, its photodynamic and photothermal activities were intensely evaluated. Moreover, its bactericidal efficiency was assessed *via in vitro* antibacterial assays and bacterial biofilm destruction tests. First, the obtained BSA@ICG@Bac showed both good singlet oxygen generation property and high photothermal conversion efficiency. In addition, it showed enhanced photodynamic and photothermal antibacterial capacities and biofilm-removing ability *in vitro* due to Bac modification. To sum up, our research provided an economic and less-time-consuming approach to preparing antibacterial nanomedicines with excellent antibacterial ability. Therefore, the prepared antibacterial nanomedicines have great potential to be utilized in clinical trials in the future.

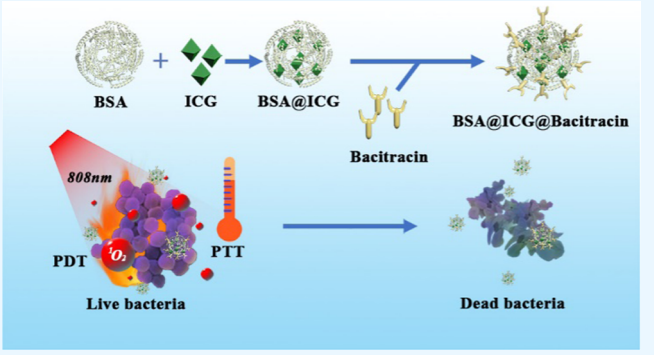

1. INTRODUCTION

With the increasing application of traditional antibiotics, bacterial drug resistance is becoming a significant threat.[1] Bacteria use various strategies to avoid the antibiotic effectiveness. For example, β-lactamases in bacteria negate the antibacterial effects of penicillin.[2] In addition, the formation of a biofilm increases the risk of treatment failure. Biofilms can provide a suitable microenvironment for bacteria, which is very unfavorable to some antibacterial agents and greatly weakens their function.[3] Rapidly increasing antibiotic resistance and high mortality rates lead to an urgent need for new alternatives in infection therapy.

Among many new antibacterial strategies, light-based local therapies such as photodynamic therapy (PDT) and photothermal therapy (PTT) emerged as alternative and complementary therapeutic methods.[4−8] Photodynamic therapy (PDT) is a kind of treatment that can kill cells with a photosensitizer and a specific wavelength laser. PDT utilizes reactive singlet oxygen ($^1O_2$) produced by photosensitizers to cause irreparable oxidative damage to vital cellular components, such as lipids, proteins, and DNA, which leads to the death of bacteria with negligible bacterial resistance.[9−14] During antibacterial therapy, irradiating the infected site with a specific wavelength can activate the photosensitive drugs selectively gathered in the infected tissue, which could induce a luminescent chemical reaction and kill the bacteria. Specifically, the activated photosensitizer can transfer energy to the surrounding oxygen and produce singlet oxygen with strong activity. Singlet oxygen can oxidize biomacromolecules, induce cytotoxicity, and then kill the bacteria.[15] Photosensitizers are pivotal in photodynamic therapy. There are many kinds of photosensitizers, such as porphyrin compounds and phthalocyanine compounds.[16] Photothermal therapy is a method that converts light energy into heat energy by photothermal conversion agents and kills bacteria by causing thermal damage to cell walls, proteins, and enzymes.[17] Currently, there are many photothermal agents. Inorganic precious metals (Ag, Au, Pt), sulfide/oxidized metals (MoS_2, CuS, MnO_2), and carbon-based nanomaterials show high photothermal conversion efficiency, which is beneficial to the application of photothermal therapy.[18]

However, some pathogenic infections occur in a hypoxic environment, or after PDT treatment, the surrounding oxygen is decreased and the reactive oxygen species (ROS) is

Received: April 20, 2022
Accepted: August 18, 2022
Published: September 16, 2022

ACS Publications

© 2022 The Authors. Published by American Chemical Society

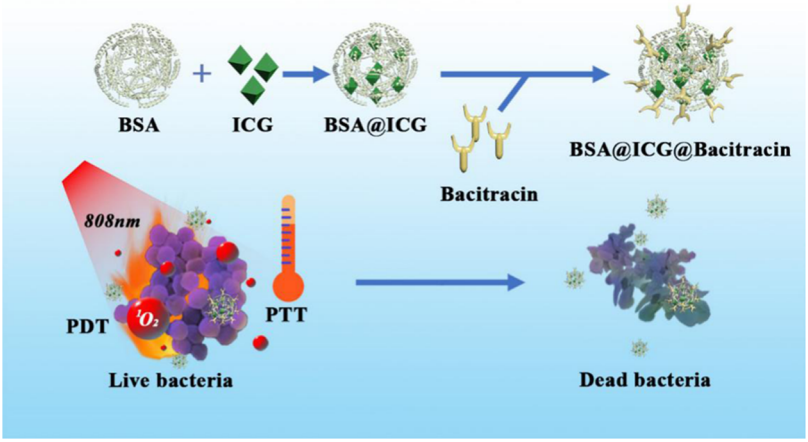

Figure 1. Schematic illustration of the construction of BSA@ICG@Bac nanomedicine for combined photothermal and photodynamic antibacterial therapy.

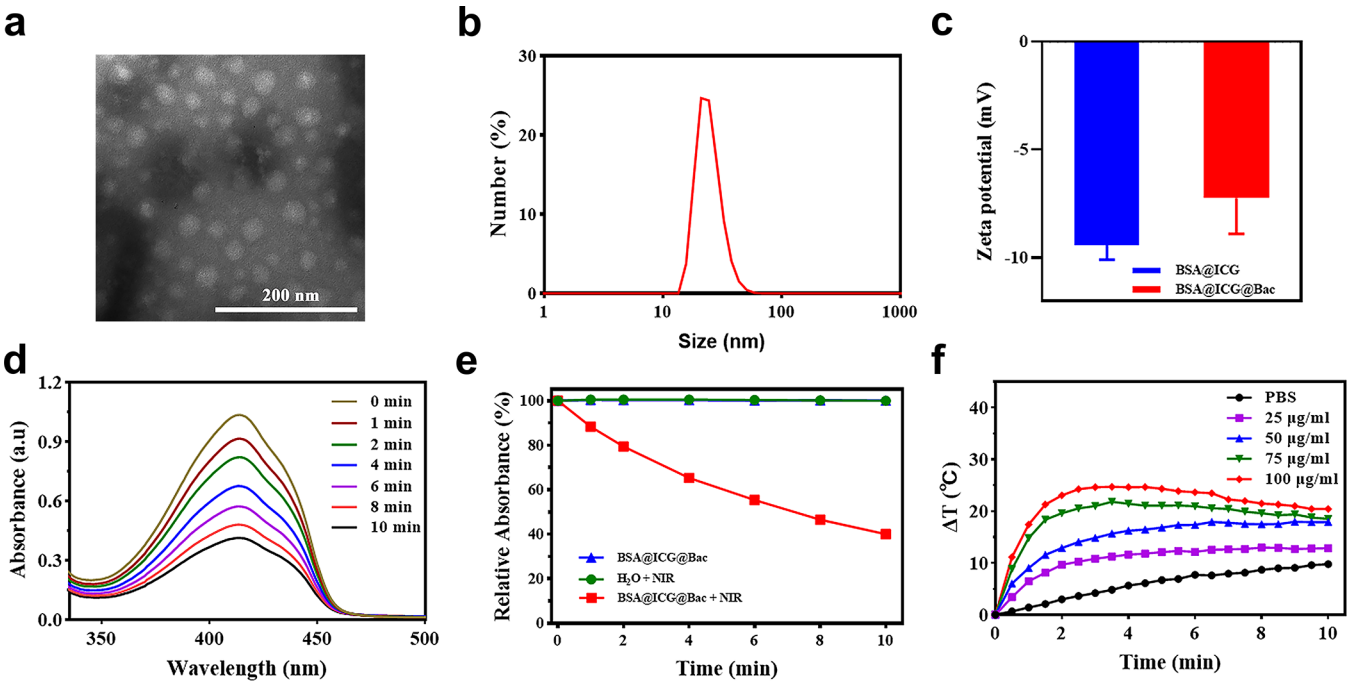

Figure 2. (a) TEM image of the BSA@ICG@Bac nanoparticle. Scale bar is 200 nm. (b) Size distributions. (c) ζ potentials of diverse drug-loaded nanoparticles (BSA@ICG and BSA@ICG@Bac). (d) Spectrogram of UV absorption of 1,3-diphenylisobenzofuran (DPBF) with BSA@ICG@Bac under 808 nm irradiation. (e) Absorption strength of the different sample groups. (f) Photothermal conversion curves of BSA@ICG@Bac at 1 W/cm^2.

insufficient, which seriously affect the antibacterial effect of PDT.[19] In addition, due to the poor penetration of white light in the tissue, the use of visible light to PDT limits the therapeutic effect of bacterial infection in deep tissues.

In addition, the thermal effect produced by photothermal therapy is poorly specific to bacteria, which can easily attack the surrounding cells and tissues. Meanwhile, the agents for photothermal therapy and photodynamic therapy often showed low biocompatibility and difficult biodegradation. Also, some new agents with complex synthesis processes were also not suitable for further development.[20]

To improve the antibacterial ability of these light-based local therapies and avoid the defects caused by the unilateral application of photodynamic therapy or photothermal therapy, the combination of PDT and PTT to design an antibacterial system has been studied.[21−27] Recent studies showed that indocyanine green (ICG) could produce the photodynamic effect and the photothermal conversion effect at the same time at an 808 nm laser irradiation. However, as a near-infrared organic dye, ICG showed poor biocompatibility, low stability in aqueous solutions, and photobleaching and could be removed quickly *in vivo*, which limited its application.[28]

Physically coating nanomedicines with oppositely charged antibacterial peptides is an economic, versatile, and less-time-consuming approach to preparing bacterial-targeting drug delivery vehicles. Herein, to improve the poor biocompatibility and difficult biodegradation of ICG, we loaded the photosensitizer ICG onto bovine serum albumin (BSA) and modified bacitracin onto the surface of nanoparticles to form BSA@ICG@BAC nanoparticles. BSA has good biocompatibility and biodegradability. ICG is a photosensitizer that shows a good phototherapeutic effect and excellent safety clinically

https://doi.org/10.1021/acsomega.2c02470
ACS Omega 2022, 7, 33821−33829

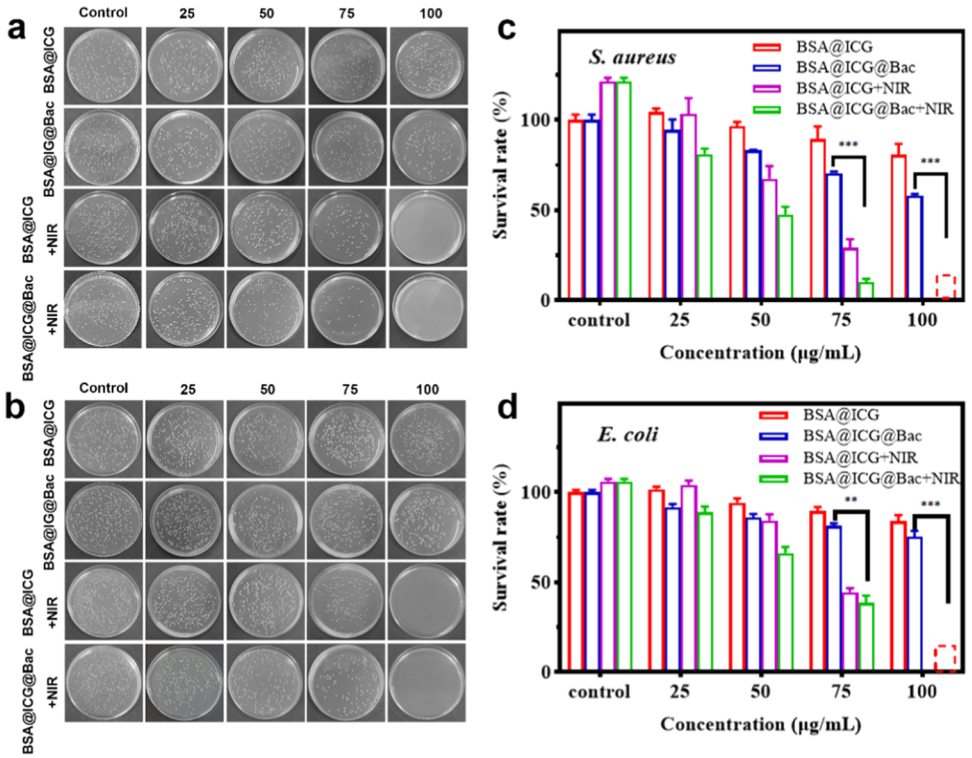

Figure 3. Photographs of bacterial colonies formed by (a) *S. aureus* and (b) *E. coli* treated with different concentrations of BSA@ICG and BSA@ICG@Bac with or without NIR (808 nm, 1 W/cm^2). The bacterial survival of (c) *S. aureus* and (d) *E. coli* after treatment as determined by the plate counting method.

approved by FDA. To augment the bacterial selectivity of the nanosystem and reduce the side effects of PTT, we modified bacitracin to the surface of nanoparticles. Bacitracin can play a certain role in bacterial targeting and bacterial killing and strengthen the antibacterial ability of the system (Figure 1).

2. RESULTS AND DISCUSSION

2.1. Synthesis and Characterization of BSA@ICG@Bac Nanoparticles. Accordingly, self-assembled BSA could be carried with ICG to obtain stable BSA@ICG nanoparticles.[32] Moreover, due to the electrostatic interaction in albumin, the Bac was attracted to the surface of BSA@ICG nanoparticles to obtain BSA@ICG@Bac nanoparticles, which was fully characterized by transmission electron microscopy (TEM), dynamic light scattering (DLS), Fourier transform infrared (FTIR) spectroscopy, and a UV−visible spectrophotometer (Figures 2a−c and S1−S3) The morphology and hydrodynamic size of the BSA@ICG@Bac nanoparticles were confirmed by transmission electron microscopy (TEM) and dynamic light scattering (DLS), respectively (Figure 2). Spherical BSA@ICG@Bac nanoparticles that were uniform and exhibited excellent stability were observed through TEM, and their average diameter was about 15.9 ± 1.7 nm (Figure 2a). Consistent with the TEM data, the average hydrodynamic diameter of BSA@ICG@Bac was 43.5 ± 2.2 nm, which was larger than the 21.3 ± 0.7 nm of BSA@ICG (Figures 2b and S1a). The BSA@ICG nanoparticles showed electronegativity in water, which was reduced after loading with electropositive Bac on its surface, implying the successful loading of the Bac (Figure 2c). The DLS measurement of BSA@ICG@Bac was performed for 7 days both in water and in phosphate-buffered saline (PBS) (pH 7.4); the hydrodynamic size of BSA@ICG@Bac was still less than 100 nm, which proved its good aqueous stability (Figure S1b,c). Moreover, the loading capacity (LC) and encapsulation efficiency (EE) were determined to be 6.6 and 80.5%, respectively (Figure S3).

2.2. Photothermal and Photodynamic Behaviors of BSA@ICG@Bac Nanoparticles. ICG, an FDA-approved drug, could generate singlet oxygen and heat after 808 nm near-infrared laser irradiation.[33] The singlet oxygen generation capability of BSA@ICG@Bac was determined by a fluorescence indicator 1,3-diphenylisobenzofuran (DPBF).[29] The more the singlet oxygen generated, the more the fluorescence decreased. In the presence of H_2O or BSA@ICG@Bac, the fluorescence of DPBF did not change without near-infrared (NIR) laser irradiation owing to the fact that no singlet oxygen was generated (Figure S4). Nevertheless, after being irradiated with an NIR laser (808 nm, 1 W/cm^2) for 10 min, the fluorescence of DPBF decreased to 40% in the presence of BSA@ICG@Bac, which confirmed that singlet oxygen was generated (Figure 2d,e). In addition, BSA@ICG@Bac generated less $^1O_2$ than free ICG under NIR irradiation. However, BSA@ICG@Bac achieved a much longer photodegradation period than free ICG (2 min), which is beneficial for photothermal therapy (Figure S5a). In comparison, we performed the $^1O_2$ generation experiment using DPBF as a probe under visible-light (660 nm) irradiation. As can be seen from Figure S5b, BSA@ICG@Bac generated less $^1O_2$ under visible-light (660 nm) irradiation than under NIR (808 nm) irradiation.

According to Figure S6, the photothermal conversion efficiency (η) of the BSA@ICG@Bac NPs at 808 nm was calculated to be 33.07%. Besides, the BSA@ICG@Bac nanoparticles exhibited excellent photothermal properties after NIR laser irradiation (808 nm, 1 W/cm^2) (Figures 2f

https://doi.org/10.1021/acsomega.2c02470
ACS Omega 2022, 7, 33821−33829

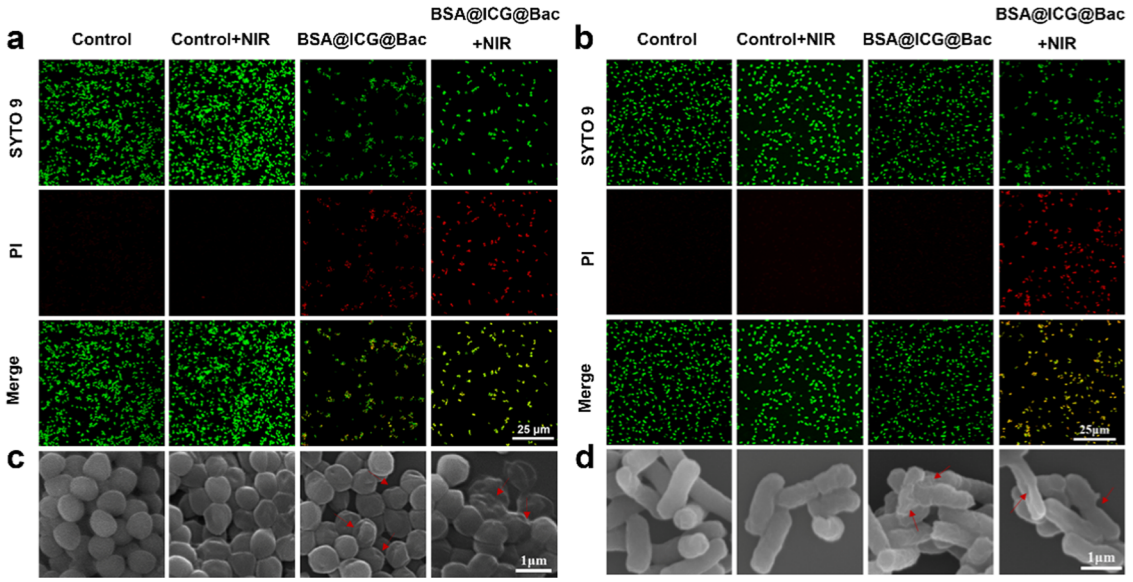

Figure 4. Fluorescence micrographs of SYTO 9 and PI-costained (a) *S. aureus* and (b) *E. coli* after various treatments. Scanning electron microscopy (SEM) images of (c) *S. aureus* and (d) *E. coli* after different treatments. Scale bar: (a, b): 25 μm; (c, d): 1 μm.

and S7). As the concentration of BSA@ICG@Bac nanoparticles increased from 25 to 100 μg/mL, the temperature increased dose-dependently. At the concentration of 100 μg/mL, the aqueous solution of BSA@ICG@Bac could heat up 24.7 °C after 3.5 min of irradiation, while the temperature of its PBS solution and at the concentration of 25 μg/mL just heated up to 5.5 and 11.2 °C, respectively (Figure 2f). With the irradiation time increasing, the temperature increase was slow or even decreased because the ICG was deactivated after NIR laser irradiation.[32,34] Taken together, BSA@ICG@Bac nanoparticles could provide both photodynamic and photothermal therapy with a single NIR laser.

2.3. *In Vitro* Antibacterial Assay. The antibacterial effects of BSA@ICG and BSA@ICG@Bac nanoparticles were assessed by a standard broth microdilution method.[30] After being incubated with different concentrations of different nanoparticles, *Staphylococcus aureus* and *Escherichia coli* were treated with or without 808 nm NIR irradiation. Due to the bacteriostatic and targeting effects of Bac, the antibacterial ability of BSA@ICG@Bac was better than that of BSA@ICG (Figure 3a,b). Notably, at the concentration of 75 μg/mL, little *S. aureus* colonies were grown on the plate with the BSA@ICG + NIR and BSA@ICG@Bac + NIR. The survival rates were 29.2% (BSA@ICG + NIR) and 10.2% (BSA@ICG@Bac + NIR), respectively (Figure 3c). In accordance with the results of *S. aureus*, the survival rates were 44.5% (BSA@ICG + NIR) and 38.5% (BSA@ICG@Bac + NIR) in *E. coli*, respectively (Figure 3d). Encouragingly, when the concentration of BSA@ICG and BSA@ICG@Bac nanoparticles was increased to 100 μg/mL, all bacteria colonies were inhibited under 808 nm NIR irradiation. In comparison, the *in vitro* antibacterial ability of BSA@ICG@Bac under visible-light (660 nm) irradiation was also evaluated. Compared with NIR (808 nm) irradiation, visible-light (660 nm) irradiation led to a dramatic decrease in the antibacterial ability at the concentration of 100 μg/mL (Figure S8). Moreover, the minimum inhibitory concentrations (MICs) of BSA@ICG@Bac for *S. aureus* and *E. coli* were determined to be 100 μg/mL with NIR irradiation (Table S1).

Meanwhile, all live/dead bacteria under different conditions were analyzed by SYTO 9 and propidium iodide (PI), which provide green fluorescence (live bacteria) and red fluorescence (dead bacteria), respectively (Figure 4a,b).[35] Consistent with the colonies on the plate, the majority of the bacteria emitted green fluorescence without any nanomaterials. Nevertheless, there was a small percentage of bacteria that emitted red fluorescence in the BSA@ICG@Bac nanoparticle group. Even more encouraging, most of the bacteria were dead, as evidenced by the emission of red fluorescence in the presence of BSA@ICG@Bac nanoparticles and NIR laser irradiation.

To further confirm the antibacterial effect and the underlying mechanism of BSA@ICG@Bac nanoparticles, scanning electron microscopy (SEM) was used.[31] Figure 4c,d shows that untreated bacteria exhibited a smooth surface with an integrated membrane structure. For the PBS + NIR and BSA@ICG@Bac groups, there were a few shrinkages on the surface of bacteria, indicating NIR irradiation or BSA@ICG@Bac nanoparticles were useless to disrupt the cell membrane. However, under 808 nm NIR irradiation, BSA@ICG@Bac nanoparticle treatment impaired the bacterial cell membrane, which shrank and collapsed, and the bacteria could barely grow on the agar plate. Therefore, nanomaterials may induce bacterial death by destroying the bacterial membranes.

To study the targeting capacity of the BSA@ICG@Bac in *S. aureus*, the uptake percentage of the nanoparticle method was used. As shown in Figure S9, the uptake proportion of nanoparticles increased in a time-dependent manner. After coincubation for 1 h, about 18.5% BSA@ICG@Bac was taken up, whereas only 14.1% BSA@ICG was taken up by *S. aureus*. Up to 210 min, 24.5% BSA@ICG@Bac was taken up by *S. aureus*, which is more than the absorptivity of BSA@ICG (21.3%). Therefore, Bac seemed to enhance the targeting capacity of nanoparticles in *S. aureus*. On the other hand, the intracellular ROS generation experiment in *S. aureus* after incubating with BSA@ICG and BSA@ICG@Bac using 2′,7′-dichloroacetate (DCFH-DA) as a probe was performed. As can be seen from Figure S10, both BSA@ICG and BSA@ICG@Bac groups generated ROS inside *S. aureus*, which confirms its antibacterial mechanism.

https://doi.org/10.1021/acsomega.2c02470
ACS Omega 2022, 7, 33821−33829

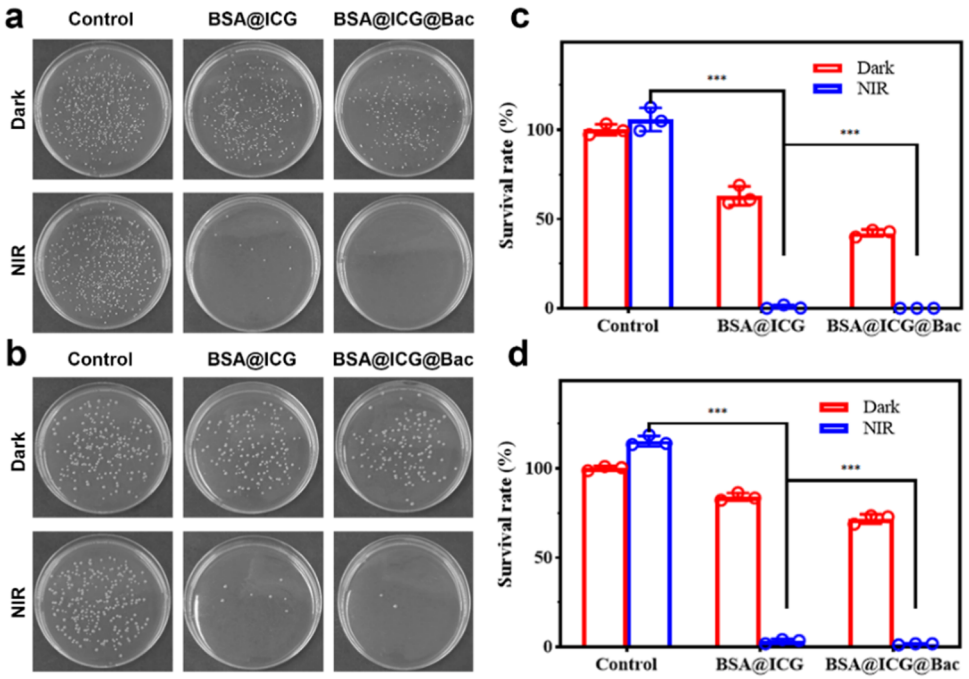

Figure 5. Plates of (a) *S. aureus* and (b) *E. coli* from the remaining cell biofilm with different treatments. The survival of (c) *S. aureus* and (d) *E. coli* after incubation with PBS, BSA@ICG, and BSA@ICG@Bac under or without NIR irradiation.

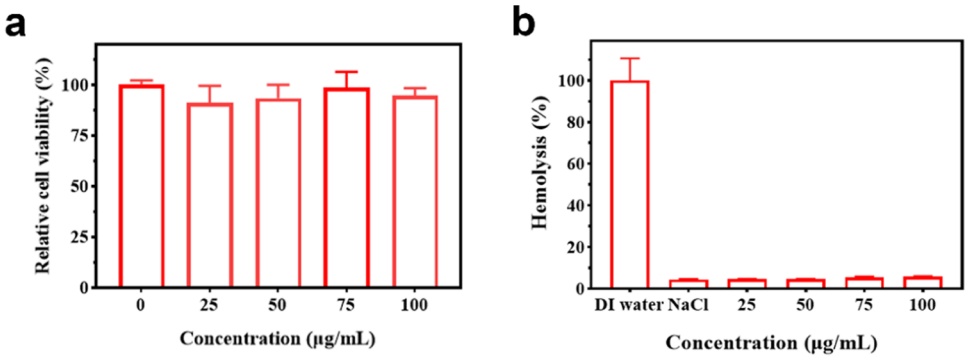

Figure 6. (a) Cell viability of L929 cells after incubation with BSA@ICG@Bac at different concentrations. (b) Relative hemolysis ratios of water, NaCl, and different concentrations of BSA@ICG@Bac.

2.4. *In Vitro* Bacterial Biofilm Destruction Test. The formation of a bacterial biofilm makes bacteria immune to the interference of the external environment such as antibiotics, light, and heat, which may cause bacterial resistance and the failure of antibiotic treatment. Thus, the treatment of bacterial infection was facing great challenges. Therefore, there is an urgent need to find a new antimicrobial strategy, especially to eliminate the formation of biofilms.

In our study, we tested bacterial biofilm destruction experiments with the intact biofilm of *S. aureus* and *E. coli*.

First, to evaluate the complete development of the bacterial biofilm, crystal violet staining was used (Figure S11). *S. aureus* and *E. coli* were incubated with PBS, BSA@ICG, and BSA@ICG@Bac in the presence or absence of NIR laser irradiation. After that, the plate counting method was used to evaluate the bacterial survival rate of the treated biofilm. As shown in Figure 5, in the BSA@ICG- or BSA@ICG@Bac-treated group, the *S. aureus* survival rates of the remaining biofilm were 63 and 42%, whereas the *E. coli* survival rates were 84 and 71%, respectively. These results suggested that the nanomaterial could destroy and penetrate the biofilm. In our study, we performed bacterial biofilm destruction experiments with the intact biofilm of *S. aureus* and *E. coli*. At the same time, under the NIR laser irradiation, the *S. aureus* and *E. coli* survival rates were 0 and 1.57% in the presence of BSA@ICG@Bac, which was lower than 0.71 and 3.72% in the presence of BSA@ICG. These data confirmed that NIR laser played an important role in antibiofilm activity, which could induce ICG to generate $^1O_2$ and heat to attack the biofilm and cause bacterial death.

2.5. *In Vitro* Biocompatibility Assay. To evaluate the *in vitro* biocompatibility assays of BSA@ICG@Bac nanoparticles, the 3-(4,5-dimethylthiazol-2-yl)-2,5-diphenyltetrazolium bromide (MTT) assay and hemolysis experiments were applied. The cytotoxicity of BSA@ICG@Bac nanoparticles (0−100 μg/mL) was determined by the MTT assay using L929 cells. As shown in Figure 6a, after 48 h of incubation, the cells of each group grew well, and the cell viability was above 90%, which indicated no potential cytotoxicity of BSA@ICG@Bac against L929 cells. At the concentration of BSA@ICG@Bac under 75 μg/mL, the cell proliferation effect of BSA was greater than its ability to inhibit cell proliferation. However, at the concentration of BSA@ICG@Bac above 75 μg/mL, the

https://doi.org/10.1021/acsomega.2c02470
ACS Omega 2022, 7, 33821−33829

toxicity of nanoparticles was so great that the cell proliferation was limited. In hemolysis assays, the test was accessed by mouse red blood cells (4%), which were coincubated with a series of gradient concentrations of BSA@ICG@Bac (0, 25, 50, 75, 100 μg/mL). Figure 6b shows that the hemolysis rate increased in a dose-dependent manner. Encouragingly, the hemolysis rate was 4.7% at the concentration of BSA@ICG@Bac of 100 μg/mL, which was less than the permissible limit (5%). Consequently, the obtained BSA@ICG@Bac nanoparticles exhibited excellent biosafety.

3. CONCLUSIONS

In conclusion, a bacterial-targeting nanomedicine, BSA@ICG@Bac NPs, was developed for antibacterial therapy. BSA@ICG@Bac NPs were conveniently produced by a thorough hydrophobic-interaction-induced self-assembly between ICG and BSA, followed by the physical immobilization of oppositely charged Bac to the surface of BSA@ICG NPs. Due to the Bac-mediated bacterial-targeting property, *in vitro* antibacterial assays demonstrated that the therapeutic efficiency of BSA@ICG@Bac NPs against both planktonic bacteria and biofilms was significantly enhanced under the irradiation of an 808 nm laser compared to BSA@ICG NPs. *In vitro* experiments proved that BSA@ICG@Bac NPs also demonstrated excellent biosafety. Therefore, this bacterial-targeting nanomedicine is a promising candidate for clinical trials in the future.

4. EXPERIMENTAL SECTION

4.1. Materials. Bovine serum albumin (BSA) was supplied by Shanghai Yuanye Biology Science and Technology Co., Ltd. (China). Indocyanine green (ICG) was provided by Meryer (Shanghai, China). Bacitracin, dimethyl sulfoxide (DMSO), and *N*,*N*-dimethylformamide (DMF) were purchased from Macklin (Shanghai, China). Luria-Bertani (LB) broth was obtained from Solarbio Reagent Co., Ltd (China). Mueller Hinton Agar was supplied by Huangdong huankai microbial SCI. & Tech Co., Ltd. (China). Dulbecco's modified Eagle's medium (DMEM) and fetal bovine serum (FBS) were purchased from Gibco. Propidium iodide (PI) was purchased from Sigma Co., Ltd. All solvents and chemicals were of analytical grade and used as received unless specified otherwise.

4.2. Synthesis of BSA@ICG@Bac Nanoparticles. To prepare BSA@ICG nanoparticles, 67 mg of BSA was dissolved in 20 mL of distilled water, and a solution of ICG (12 mg) in DMSO (8 mL) was added slowly at the rate of 1 mL/min. Then, the mixture was stirred in the dark for 12 h and dialyzed against distilled water for 24 h to obtain the aqueous solution of BSA@ICG nanoparticles. Next, 2 mL of the solution was lyophilized and weighed for measurement of the concentration. Another 2 mL of the solution was separated by ultrafiltration using Nanosep centrifugal devices with a molecular weight cutoff of 300 kD (Pall Life Sciences, Ann Arbor, MI), and the aqueous phase was kept to determine the concentration of free ICG *via* UV−vis spectroscopy in the following step.

To prepare BSA@ICG@Bac nanoparticles, bacitracin (1 mg) dissolved in deionized water (1 mL) was slowly added to the solution of BSA@ICG nanoparticles. The obtained mixture was stirred for 12 h to generate BSA@ICG@Bac nanoparticles. Then, it was dialyzed against deionized water for 24 h to obtain the aqueous solution of BSA@ICG@Bac nanoparticles. Then, 2 mL of the solution was lyophilized and weighed for measurement of the concentration.

4.3. Instrument. Dynamic light scattering (DLS) was measured by a Zetasizer nanoZS (Horiba SCI. Ltd., Japan) for the ζ potential and size distribution of nanoparticles in distilled water. A transmission electron microscope (TEM) image was obtained by JEM-1400 (Japan) at 80 kV. The UV−vis absorption was recorded by a UV−visible spectrophotometer (UV-6000PC, Shanghai Metash instruments Co., Ltd.). A scanning electron microscope (SEM, Zeiss Gemini SEM 300) was used to observe the morphology of bacteria. Fluorescence images were obtained by confocal laser scanning microscopy (Leica, SP8, Germany). Fourier transformed infrared (FTIR) spectra were obtained by the KBr pellet method in an FTIR spectrophotometer (Bruker, TENSOR 27, Germany).

4.4. Measurement of the ICG Loading Amount in BSA@ICG@Bac Nanoparticles. In our work, UV−vis spectroscopy was used to determine the loading capacity (LC) and encapsulation efficiency (EE) of the content of ICG in the final formulation of BSA@ICG@Bac. The aqueous phase (0.4 mL) kept during the preparation of BSA@ICG was dissolved in the cosolvent system of DMSO/H_2O (1:5, v/v, 2 mL) for UV−vis measurement at the wavelength of 783 nm to determine the concentration of unloaded ICG. The LC and EE of BSA@ICG@Bac were calculated according to the following formula

$$\mathrm{LC}\ (\%) = (W_T - W_F)/W_{NP} \times 100\% \quad (1)$$

where W_T is the total weight of the drug fed, W_F is the weight of the nonencapsulated free drug, and W_{NP} is the weight of drug-loaded nanoparticles.

$$\mathrm{EE}\ (\%) = (W_T - W_F)/W_T \times 100\% \quad (2)$$

where W_T is the total weight of the drug fed and W_F is the weight of the nonencapsulated free drug.

4.5. Photothermal Performance of BSA@ICG@Bac Nanoparticles. To verify the photothermal effect of BSA@ICG@Bac nanoparticles, an infrared thermal imaging camera was used to document the temperature changes of various concentrations (25, 50, 75, 100 μg/mL) of nanoparticles (1 mL) under an 808 nm NIR laser (1 W/cm^2) irradiation (Zhongjiao Jinyuan Technology, 16 Ltd., Beijing, China).

4.6. Detection of $^1O_2$ Generation. The production of $^1O_2$ was analyzed using the method described previously.[28] Briefly, 700 μL of DMF and 300 μL of distilled water were added into a Quartz cuvette as a negative group. Then, 290 μL of free ICG and BSA@ICG@Bac (100 μg/mL) with an equal concentration of ICG were mixed with 10 μL of a 5 mM DPBF solution and 700 μL of DMF in the miscible liquids. Finally, the whole solution was exposed to 808/660 nm LED irradiation for different times (0, 1, 2, 4, 6, 8, and 10 min), and the absorbance was recorded by UV−vis spectroscopy.

4.7. Bacteria Culture. Single colonies of *S. aureus* (ATCC 25923) and *E. coli* (ATCC 25922) on a solid Mueller Hinton (MH) agar plate were dispersed in 5 mL of LB, separately, and cultured at 37 °C under 110 rpm shaking overnight. The bacteria were centrifuged and washed with 0.9% NaCl, which were resuspended in fresh LB.

4.8. *In Vitro* Antibacterial Study. *S. aureus* or *E. coli* (100 μL, 10^7 CFU/mL) was added to a 96-well plate for different treatments. They were incubated with PBS, BSA@ICG (100, 75, 50, 25 μg/mL, 100 μL), and BSA@ICG@Bac (100, 75, 50, 25 μg/mL, 100 μL) for 3 h, separately. Then, they were treated

https://doi.org/10.1021/acsomega.2c02470
ACS Omega 2022, 7, 33821−33829

with or without 808 nm laser irradiation for 10 min. Finally, a method of colony counting using solid agar plates was employed to evaluate the antibacterial property of the material.[30] In addition, the same method was used to treat bacteria under 660 nm LED for 10 min as a comparison.

The minimum inhibitory concentrations (MICs) of NPs against *S. aureus* and *E. coli* were determined by a previously reported method.[36] BSA@ICG and BSA@ICG@Bac NPs were serially diluted 2-fold in LB in 96-well plates to obtain concentrations ranging from 25 to 400 μg/mL. The endpoints were determined when no turbidity in the well was observed.

4.9. Scanning Electron Microscopy Characterization. To visualize the influence of materials on bacteria, a bacterial solution (10^8 CFU/mL, 500 μL) was mixed with PBS (pH ∼ 7.4) or BSA@ICG@Bac NPs (200 μg/μL, 500 μL) in a 48-well plate. After incubating for 3 h at 37 °C, the group NIR(+) was exposed to 808 nm laser irradiation (1 W/cm^2) for 10 min, while the group NIR(−) was kept in the dark. After that, the bacteria were resuspended in a glutaraldehyde solution (2.5%) and fixed for 12 h at 4 °C. Then, the bacteria were dehydrated with different concentrations of ethanol (30, 50, 70, 80, 90, 100%) for 10 min, separately. After drying with a vacuum dryer overnight and sputter-coating with platinum for 60 s, the samples were obtained and visualized by SEM.[16]

4.10. *In Vitro* Bacterial Biofilm Destruction Test. The bacterial biofilms (*E. coli* and *S. aureus*) were constructed by culturing the bacteria into a tryptic soy broth (TSB) medium at a concentration of 10^9 CFU/mL for 48 h at 37 °C with a constant agitation speed of 110 rpm. The obtained biofilms were treated differently, and they were divided into six groups: (a) control; (b) control + NIR; (c) BSA@ICG (100 μg/μL); (d) BSA@ICG (100 μg/μL) + NIR; (e) BSA@ICG@Bac (100 μg/μL); and (f) BSA@ICG@Bac (100 μg/μL) + NIR. After treatment, the 48-well plate was ultrasonicated for 10 min to disperse the remaining biofilms into the solution. Finally, the method of colony counting using solid agar plates was employed to determine the CFU in biofilms.

4.11. Live/Dead Bacterial Staining Assay. The bacteria (*E. coli* and *S. aureus*, 10^7 CFU/mL) were cultured with PBS and BSA@ICG@Bac at 37 °C for 3 h. The group NIR(+) was exposed to an 808 nm laser irradiation (1 W/cm^2) for 10 min, while the group NIR(−) was kept in the dark. After centrifugation and washing with PBS, SYTO 9 (0.6 μL, 1.5 mM) and propidium iodide (PI, 1 μL, 1.5 mM) were sequentially mixed with a bacterial suspension (100 μL) in the dark for 20 min. After centrifugation, the stained bacteria were resuspended in PBS for confocal laser scanning microscope (CLSM, Leica, SP8) measurement. SYTO 9 and PI were excited at 488 and 561 nm, and the emission signals were collected at 500−545 nm (green channel) and 600−650 nm (red channel), respectively.

4.12. Bacterial Uptake of BSA@ICG@Bac. BSA@ICG and BSA@ICG@Bac (1 mL, 100 μg/mL) were added to the bacterial solution (1 mL, 2×10^8 CFU/mL) in a 24-well plate and cultured at 37 °C at a shaking speed of 100 rpm for different time intervals (60, 90, 120, 150, 180, and 210 min). After centrifugation, the pellet was washed gently with PBS to remove the unbound BSA@ICG or BSA@ICG@Bac. Then, it was incubated with methanol (300 μL) at room temperature for 2 h and centrifuged at 5000 rpm for 10 min. The absorbance of the supernatant at 783 nm was measured to evaluate the bacterial uptake capacity of BSA@ICG@Bac according to the following formula

$$\text{uptake of ICG (\%)} = [M_1/M_0] \times 100\% \quad (3)$$

where M_1 is the amount of ICG in the supernatant and M_0 stands for the total amount of ICG in BSA@ICG or BSA@ICG@Bac.

4.13. *In Vitro* Cytotoxicity Assays. The MTT assay was used to measure the cytotoxicity of BSA@ICG@Bac nanoparticles. L929 cells were grown in DMEM supplemented with 10% FBS and 1% penicillin/streptomycin. BSA@ICG@Bac (100, 75, 50, 25 μg/mL) was coincubated with L929 cells (5000 cells per well) in a 96-well plate at 37 °C in a 5% CO_2 atmosphere for 24 h, separately. After that, 10 μL of MTT (5 mg/mL) was added to each well and incubated for 4 h. Then, the supernatant was removed, and DMSO (100 μL) was added to each well for incubation (15 min) and shaking. The relative cell viability was calculated by measuring the absorbance at 570 nm.

4.14. Hemolysis Assays. Hemolysis was characterized by rat red blood cells (RBCs) from BALB/c mouse. The whole blood (1 mL) was added to 0.9% NaCl (9 mL) solution, and RBCs were obtained by centrifuging at 750 rpm for 10 min and washed until the supernatant was clear. Then, 400 μL of BSA@ICG@Bac (200, 150, 100, 50 μg/mL) was mixed with 400 μL of 4% v/v RBCs and incubated for 1 h at 37 °C, separately. After centrifuging at 1000 rpm for 5 min, the supernatants (100 μL) were transferred to a 96-well plate for UV−vis measurement at the wavelength of 576 nm using a microplate reader (Biotek). The dispersions of RBCs incubated with DI water and 0.9% NaCl were used as the positive and negative controls, separately. The hemolysis rate of BSA@ICG@Bac nanoparticles can be calculated from the following formula

$$\text{hemolysis ratio (\%)} = (A_{\text{sample}} - A_{\text{N}})/(A_{\text{P}} - A_{\text{N}}) \times 100\% \quad (4)$$

where A_{sample} is the absorbance of RBCs incubated with BSA@ICG@Bac nanoparticles, A_{N} reflects the absorbance of RBCs incubated with 0.9% NaCl, and A_{P} stands for the absorbance of RBCs incubated with DI water.

4.15. Detection of Intracellular Reactive Oxygen Species (ROS). 2′,7′-Dichloroacetate (DCFH-DA) was used to detect the ROS produced.[37] Briefly, the overnight test culture (1×10^7 CFU/mL) was treated with BSA@ICG and BSA@ICG@Bac in an appropriate concentration and preincubated for 4 h. The preincubated samples were treated with 100 μM DCFH-DA and incubated in the dark for 30 min. Excess of DCFH-DA from the samples was removed by centrifugation and irradiated for 10 min. The control wells were maintained untreated. A similar experiment was maintained in the dark for comparison. CLSM was used to observe the bacteria (ex = 488 nm, em = 525 nm).

4.16. Statistical Analysis. The values were manifested as mean ± standard deviation (SD), and the data were gathered based on more than three parallel experiments. The statistical analysis was concluded using Student's *t*-test. In all tests, the statistical significance for the test was set at $*p < 0.05$, $**p < 0.01$, and $***p < 0.001$.

■ ASSOCIATED CONTENT

Supporting Information

The Supporting Information is available free of charge at https://pubs.acs.org/doi/10.1021/acsomega.2c02470.

Particle size distribution of BSA@ICG, and stability of BSA@ICG@Bac in water and PBS 7.4 (Figure S1); drug

https://doi.org/10.1021/acsomega.2c02470
ACS Omega 2022, 7, 33821−33829

loading of ICG in BSA@ICG@Bac (Figure S2); effect of water on the UV−vis absorption spectrum of DPBF under 808 nm laser irradiation and the effect of BSA@ICG@Bac in the dark (Figure S3); absorption intensity under different conditions (Figure S4); photothermal conversion efficiency of BSA@ICG@Bac (Figure S5); FTIR spectra of the raw materials forming BSA@ICG@Bac and BSA@ICG@Bac (Figure S6); photothermal imaging of BSA@ICG@Bac at different concentrations (Figure S7); *in vitro* antimicrobial activity of BSA@ICG and BSA@ICG@Bac with or without 660 nm laser irradiation (Figure S8); targeting of BSA@ICG and BSA@ICG@Bac by *S. aureus* (Figure S9); fluorogram of the intracellular production of reactive oxygen species by *S. aureus* (Figure S10); and photographs of *S. aureus* and *E. coli* biofilms (Figure S11) and of BSA@ICG@Bac (Table S1) (PDF)

(PDF)

AUTHOR INFORMATION

Corresponding Authors

Lijun Song − *Guangdong Key Laboratory for Research and Development of Natural Drugs, School of Pharmacy, Guangdong Medical University, Zhanjiang 524023, China*; Email: songlijun6981@126.com

Li Li − *Guangdong Key Laboratory for Research and Development of Natural Drugs, School of Pharmacy, Guangdong Medical University, Zhanjiang 524023, China*; orcid.org/0000-0002-6058-9326; Email: china_lovelylily@hotmail.com

Authors

Yueying Xu − *Guangdong Key Laboratory for Research and Development of Natural Drugs, School of Pharmacy, Guangdong Medical University, Zhanjiang 524023, China*

Wenhong Zhou − *Guangdong Key Laboratory for Research and Development of Natural Drugs, School of Pharmacy, Guangdong Medical University, Zhanjiang 524023, China*

Le Xiao − *Guangdong Key Laboratory for Research and Development of Natural Drugs, School of Pharmacy, Guangdong Medical University, Zhanjiang 524023, China*

Qian Lan − *Guangdong Key Laboratory for Research and Development of Natural Drugs, School of Pharmacy, Guangdong Medical University, Zhanjiang 524023, China*

Mingen Li − *Guangdong Key Laboratory for Research and Development of Natural Drugs, School of Pharmacy, Guangdong Medical University, Zhanjiang 524023, China*

Yun Liu − *Guangdong Key Laboratory for Research and Development of Natural Drugs, School of Pharmacy, Guangdong Medical University, Zhanjiang 524023, China*

Complete contact information is available at: https://pubs.acs.org/10.1021/acsomega.2c02470

Author Contributions

†Y.X., W.Z., and L.X. contributed equally to this work. The manuscript was written through contributions of all authors.

Notes

The authors declare no competing financial interest.

ACKNOWLEDGMENTS

This work was supported by the National Natural Science Foundation of China (Nos. 81973548 and 81473401), the Key Project of Social Science and Technology Development of Dongguan (No. 20185071521658), the Innovation and Entrepreneurship Team Leads the Pilot Program of Zhanjiang (2020LHJH005), and the Province Universities and Colleges Pearl River Scholar Fund (No. 4SG21006G).

REFERENCES

(1) Sultan, I.; Rahman, S.; Jan, A. T.; Siddiqui, M. T.; Mondal, A. H.; Haq, Q. M. R. Antibiotics, Resistome and Resistance Mechanisms: A Bacterial Perspective. *Front. Microbiol.* **2018**, *9*, No. 2066.

(2) Varela, M. F.; Stephen, J.; Lekshmi, M.; Ojha, M.; Wenzel, N.; Sanford, L. M.; Hernandez, A. J.; Parvathi, A.; Kumar, S. H. Bacterial Resistance to Antimicrobial Agents. *Antibiotics* **2021**, *10*, No. 593.

(3) Samrot, A. V.; Abubakar Mohamed, A.; Faradjeva, E.; Si Jie, L.; Hooi Sze, C.; Arif, A.; Chuan Sean, T.; Norbert Michael, E.; Yeok Mun, C.; Xiao Qi, N.; Ling Mok, P.; Kumar, S. S. Mechanisms and Impact of Biofilms and Targeting of Biofilms Using Bioactive Compounds-A Review. *Medicina* **2021**, *57*, No. 839.

(4) Şen Karaman, D.; Ercan, U. K.; Bakay, E.; Topaloğlu, N.; Rosenholm, J. M. Evolving Technologies and Strategies for Combating Antibacterial Resistance in the Advent of the Postantibiotic Era. *Adv. Funct. Mater.* **2020**, *30*, No. 1908783.

(5) Zhang, A. N.; Wu, W.; Zhang, C.; Wang, Q. Y.; Zhuang, Z. N.; Cheng, H.; Zhang, X. Z. A versatile bacterial membrane-binding chimeric peptide with enhanced photodynamic antimicrobial activity. *J. Mater. Chem. B* **2019**, *7*, 1087−1095.

(6) Jia, Q.; Song, Q.; Li, P.; Huang, W. Rejuvenated Photodynamic Therapy for Bacterial Infections. *Adv. Healthcare Mater.* **2019**, *8*, No. e1900608.

(7) Yang, H.; Liang, Y.; Wang, J.; Li, Q.; Li, Q.; Tang, A.; Liu, Y.; Liu, H. B. Multifunctional wound dressing for rapid hemostasis, bacterial infection monitoring and photodynamic antibacterial therapy. *Acta Biomater.* **2021**, *135*, 179−190.

(8) Liu, Y.; Zaat, S. A. et al. Antibacterial photodynamic therapy: overview of a promising approach to fight antibiotic-resistant bacterial infections *J. Clin. Transl. Res.* 2015, *1*, 140 167.

(9) Anas, A.; Sobhanan, J.; Sulfiya, K. M.; Jasmin, C.; Sreelakshmi, P. K.; Biju, V. Advances in photodynamic antimicrobial chemotherapy. *J. Photochem. Photobiol., C* **2021**, *49*, No. 100452.

(10) Ma, Q.; Sun, X.; Wang, W.; Yang, D.; Yang, C.; Shen, Q.; Shao, J. Diketopyrrolopyrrole-derived organic small molecular dyes for tumor phototheranostics. *Chin. Chem. Lett.* **2022**, *33*, 1681−1692.

(11) Qu, X.-Y.; Hong, Y.; Cai, H.; Sun, X.; Shen, Q.; Yang, D.-L.; Dong, X.-C.; Jiao, A.-H.; Chen, P.; Shao, J.-J. Promoted intramolecular photoinduced-electron transfer for multi-mode imaging-guided cancer photothermal therapy. *Rare Met.* **2022**, *41*, 56−66.

(12) Xiong, R.; Hua, D.; Van Hoeck, J.; Berdecka, D.; Léger, L.; De Munter, S.; Fraire, J. C.; Raes, L.; Harizaj, A.; Sauvage, F.; et al. Photothermal nanofibres enable safe engineering of therapeutic cells. *Nat. Nanotechnol.* **2021**, *16*, 1281−1291.

(13) Gao, G.; Jiang, Y. W.; Jia, H. R.; Wu, F. G. Near-infrared light-controllable on-demand antibiotics release using thermo-sensitive hydrogel-based drug reservoir for combating bacterial infection. *Biomaterials* **2019**, *188*, 83−95.

(14) Yi, X.; Duan, Q. Y.; Wu, F. G. Low-Temperature Photothermal Therapy: Strategies and Applications. *Research* **2021**, *2021*, No. 9816594.

(15) Cieplik, F.; Deng, D.; Crielaard, W.; Buchalla, W.; Hellwig, E.; Al-Ahmad, A.; Maisch, T. Antimicrobial photodynamic therapy - what we know and what we don't. *Crit. Rev. Microbiol.* **2018**, *44*, 571−589.

(16) Escudero, A.; Carrillo-Carrión, C.; Castillejos, M. C.; Romero-Ben, E.; Rosales-Barrios, C.; Khiar, N. Photodynamic therapy: photosensitizers and nanostructures. *Mater. Chem. Front.* **2021**, *5*, 3788−3812.

(17) Yougbaré, S.; Mutalik, C.; Okoro, G.; Lin, I. H.; Krisnawati, D. I.; Jazidie, A.; Nuh, M.; Chang, C. C.; Kuo, T. R. Emerging Trends in Nanomaterials for Antibacterial Applications. *Int. J. Nanomed.* **2021**, *16*, 5831−5867.

(18) Chen, Y.; Gao, Y.; Chen, Y.; Liu, L.; Mo, A.; Peng, Q. Nanomaterials-based photothermal therapy and its potentials in antibacterial treatment. *J. Controlled Release* **2020**, *328*, 251−262.
(19) Zhang, H.; Liang, Y.; Zhao, H.; Qi, R.; Chen, Z.; Yuan, H.; Liang, H.; Wang, L. Dual-Mode Antibacterial Conjugated Polymer Nanoparticles for Photothermal and Photodynamic Therapy. *Macromol. Biosci.* **2020**, *20*, No. 1900301.
(20) Deng, X.; Shao, Z.; Zhao, Y. Solutions to the Drawbacks of Photothermal and Photodynamic Cancer Therapy. *Adv. Sci.* **2021**, *8*, No. 2002504.
(21) Wang, W.; Cheng, X.; Liao, J.; Lin, Z.; Chen, L.; Liu, D.; Zhang, T.; Li, L.; Lu, Y.; Xia, H. Synergistic Photothermal and Photodynamic Therapy for Effective Implant-Related Bacterial Infection Elimination and Biofilm Disruption Using Cu9S8 Nanoparticles. *ACS Biomater. Sci. Eng.* **2019**, *5*, 6243−6253.
(22) Bilici, K.; Atac, N.; Muti, A.; Baylam, I.; Dogan, O.; Sennaroglu, A.; Can, F.; Yagci Acar, H. Broad spectrum antibacterial photodynamic and photothermal therapy achieved with indocyanine green loaded SPIONs under near infrared irradiation. *Biomater. Sci.* **2020**, *8*, 4616−4625.
(23) Yuan, Z.; Lin, C.; He, Y.; Tao, B.; Chen, M.; Zhang, J.; Liu, P.; Cai, K. Near-Infrared Light-Triggered Nitric-Oxide-Enhanced Photodynamic Therapy and Low-Temperature Photothermal Therapy for Biofilm Elimination. *ACS Nano* **2020**, *14*, 3546−3562.
(24) Liao, Z. Y.; Xia, Y. M.; Zuo, J. M.; Wang, T.; Hu, D. T.; Li, M. Z.; Shao, N. N.; Chen, D.; Song, K. X.; Yu, X.; et al. Metal-Organic Framework Modified MoS2 Nanozyme for Synergetic Combating Drug-Resistant Bacterial Infections via Photothermal Effect and Photodynamic Modulated Peroxidase-Mimic Activity. *Adv. Healthcare Mater.* **2022**, *11*, No. e2101698.
(25) Wang, R.; Kim, D.; Yang, M.; Li, X.; Yoon, J. Phthalocyanine-Assembled "One-For-Two" Nanoparticles for Combined Photodynamic-Photothermal Therapy of Multidrug-Resistant Bacteria. *ACS Appl. Mater. Interfaces* **2022**, *14*, 7609−7616.
(26) Gao, D. Y.; Ji, X.; Wang, J. L.; Wang, Y. T.; Li, D. L.; Liu, Y. B.; Chang, K. W.; Qu, J. L.; Zheng, J.; Yuan, Z. Engineering a protein-based nanoplatform as an antibacterial agent for light activated dual-modal photothermal and photodynamic therapy of infection in both the NIR I and II windows. *J. Mater. Chem. B* **2018**, *6*, 732−739.
(27) Zhang, H.; Liang, Y.; Zhao, H.; Qi, R.; Chen, Z.; Yuan, H.; Liang, H.; Wang, L. Dual-Mode Antibacterial Conjugated Polymer Nanoparticles for Photothermal and Photodynamic Therapy. *Macromol. Biosci.* **2020**, *20*, No. e1900301.
(28) Bilici, K.; Atac, N.; Muti, A.; Baylam, I.; Dogan, O.; Sennaroglu, A.; Can, F.; Yagci Acar, H. Broad spectrum antibacterial photodynamic and photothermal therapy achieved with indocyanine green loaded SPIONs under near infrared irradiation. *Biomater. Sci.* **2020**, *8*, 4616−4625.
(29) Kawasaki, H.; Kumar, S.; Li, G.; Zeng, C.; Kauffman, D. R.; Yoshimoto, J.; Iwasaki, Y.; Jin, R. Generation of Singlet Oxygen by Photoexcited Au25(SR)18 Clusters. *Chem. Mater.* **2014**, *26*, 2777−2788.
(30) Liu, Z.; Zhao, X.; Yu, B.; Zhao, N.; Zhang, C.; Xu, F. J. Rough Carbon-Iron Oxide Nanohybrids for Near-Infrared-II Light-Responsive Synergistic Antibacterial Therapy. *ACS Nano* **2021**, *15*, 7482−7490.
(31) Guo, X.; Cao, B.; Wang, C.; Lu, S.; Hu, X. In vivo photothermal inhibition of methicillin-resistant *Staphylococcus aureus* infection by in situ templated formulation of pathogen-targeting phototheranostics. *Nanoscale* **2020**, *12*, 7651−7659.
(32) Xu, L.; Wang, S. B.; Xu, C.; Han, D.; Ren, X. H.; Zhang, X. Z.; Cheng, S. X. Multifunctional Albumin-Based Delivery System Generated by Programmed Assembly for Tumor-Targeted Multimodal Therapy and Imaging. *ACS Appl. Mater. Interfaces* **2019**, *11*, 38385−38394.
(33) Yuan, Z.; Lin, C.; He, Y.; Tao, B.; Chen, M.; Zhang, J.; Liu, P.; Cai, K. Near-Infrared Light-Triggered Nitric-Oxide-Enhanced Photodynamic Therapy and Low-Temperature Photothermal Therapy for Biofilm Elimination. *ACS Nano* **2020**, *14*, 3546−3562.
(34) Sahu, A.; Lee, J. H.; Lee, H. G.; Jeong, Y. Y.; Tae, G. Prussian blue/serum albumin/indocyanine green as a multifunctional nanotheranostic agent for bimodal imaging guided laser mediated combinatorial phototherapy. *J. Controlled Release* **2016**, *236*, 90−9.
(35) Cao, B.; Xiao, F.; Xing, D.; Hu, X. Polyprodrug Antimicrobials: Remarkable Membrane Damage and Concurrent Drug Release to Combat Antibiotic Resistance of Methicillin-Resistant *Staphylococcus aureus*. *Small* **2018**, *14*, No. 1802008.
(36) Contreras Cárdenas, A. V.; Hernandez, L. R.; Juarez, Z. N.; Sanchez-Arreola, E.; Bach, H. Antimicrobial, cytotoxic, and anti-inflammatory activities of Pleopeltis polylepis. *J. Ethnopharmacol.* **2016**, *194*, 981−986.
(37) Lin, A.; Liu, Y.; Zhu, X.; Chen, X.; Liu, J.; Zhou, Y.; Qin, X.; Liu, J. Bacteria-Responsive Biomimetic Selenium Nanosystem for Multidrug-Resistant Bacterial Infection Detection and Inhibition. *ACS Nano* **2019**, *13*, 13965−13984.

https://doi.org/10.1021/acsomega.2c02470
ACS Omega 2022, 7, 33821−33829